Cryogenic high-resolution X-ray spectrometers for SR-XRF and microanalysis

M. Frank,[a]* C. A. Mears,[a] S. E. Labov,[a] L. J. Hiller,[a] J. B. le Grand,[a] M. A. Lindeman,[a] H. Netel,[a] D. Chow[a] and A. T. Barfknecht[b]

[a]Lawrence Livermore National Laboratory, PO Box 808, L-418, Livermore, CA 94551, USA, and [b]Conductus Inc., 969 West Maude Avenue, Sunnyvale, CA 94086, USA. E-mail: matt@imager.llnl.gov

Experimental results are presented obtained with a cryogenically cooled high-resolution X-ray spectrometer based on a 141 × 141 μm Nb-Al-Al$_2$O$_3$-Al-Nb superconducting tunnel junction (STJ) detector in an SR-XRF demonstration experiment. STJ detectors can operate at count rates approaching those of semiconductor detectors while still providing a significantly better energy resolution for soft X-rays. By measuring fluorescence X-rays from samples containing transition metals and low-Z elements, an FWHM energy resolution of 6–15 eV for X-rays in the energy range 180–1100 eV has been obtained. The results show that, in the near future, STJ detectors may prove very useful in XRF and microanalysis applications.

Keywords: cryogenic detectors; low-temperature detectors; microcalorimeters; X-ray fluorescence; X-ray spectroscopy.

1. Introduction

Superconducting tunnel junctions (STJs) are one prominent type of cryogenic detector, a new class of energy-resolving photon and particle detectors (Ott & Zehnder, 1996; Twerenbold, 1996; Booth & Goldie, 1996). The energy resolution of such detectors, typically operating at temperatures below ~1 K, can be at least an order of magnitude better than for conventional ionization-based semiconductor detectors such as SiLi or Ge detectors. Among the best reported photon energy resolutions achieved with STJ detectors are 29 eV (FWHM) at 6 keV (Mears *et al.*, 1996), 12.5 eV at 1 keV (Hiller *et al.*, 1995) and 1.3 eV at 3.5 eV (Peacock *et al.*, 1996). Compared with other types of cryogenic detectors, STJ detectors can count at high count rates of several 10000 counts s^{-1} because of their relatively fast (~μs) pulse decay times. In addition, the cryogenics and electronics required for operating STJ detectors are relatively simple. These properties render STJ detectors potentially interesting tools for a wide range of applications, such as X-ray fluorescence microanalysis or synchrotron radiation X-ray fluorescence.

In a previous paper (Frank *et al.*, 1998) we described the results of a detector performance study in which the STJ detector was irradiated directly with a monochromated synchrotron beam. In that study we achieved an energy resolution of 5.9 eV (FWHM) for 277 eV X-rays (the energy corresponding to C K lines) and an electronic noise of 4.5 eV at low count rates of several 100 counts s^{-1}. Increasing the count rate to 10000 counts s^{-1}, the

energy resolution of our detector at an incident energy of 277 eV remained better than 10 eV. For higher count rates the resolution degraded slowly with increasing rate to 20 eV for 277 eV X-rays at 50000 counts s^{-1}. We also found that the intrinsic energy resolution for this detector for X-rays in the range 70–700 eV scaled roughly linearly with the incident energy. Here we present experimental results obtained using the same detector in an SR-XRF demonstration experiment, also performed at the SSRL, in which we measured fluorescence X-rays from samples containing transition metals and low-Z elements.

2. Experimental details

Fig. 1 shows a schematic cross section and a schematic top view of the STJ detector, which was fabricated at Conductus Inc. using a modified photolithographic Nb trilayer process (Barfknecht *et al.*, 1991). The detector consists of a 265 nm-thick Nb base layer and a 165 nm-thick Nb counter electrode separated by a thin (~20 Å) Al$_2$O$_3$ tunnel barrier with 50 nm-thick Al 'trapping' layers on each side. The detector is diamond-shaped with an area of 141 × 141 μm. During operation, a small bias voltage ($V_{bias} \simeq 0.4$ mV) is applied across the barrier. Also, a small magnetic field ($B \simeq 100$ G) is applied parallel to the tunnel barrier and in the direction indicated in Fig. 1(b) in order to suppress the d.c. Josephson current in the device. The detector is operated at a temperature of 500 mK or below, which is well below the superconducting transition temperature of the superconducting layers. The absorption of an X-ray photon in one of the layers breaks Cooper pairs in the superconductor creating quasiparticle excitations, which can quantum mechanically tunnel through the Al$_2$O$_3$ barrier and create a measurable current pulse. The amplitude of the current pulse, typically fractions of a microampere, is proportional to the energy of the absorbed X-ray photon. The current pulse decay time is typically given by the quasiparticle lifetime of a few microseconds. The Al layers, with lower superconducting gap energy than the Nb layers, help increase the signal by concentrating quasiparticles near the tunnel barrier by means of 'quasiparticle trapping' (Booth, 1987). [For more details on the operating principle, see Mears *et al.* (1995) and Frank *et al.* (1998).] The theoretical limit for the FWHM energy resolution of an X-ray spectrometer based on the measurement of the X-ray induced quasiparticle excitations in pure Nb has been calculated
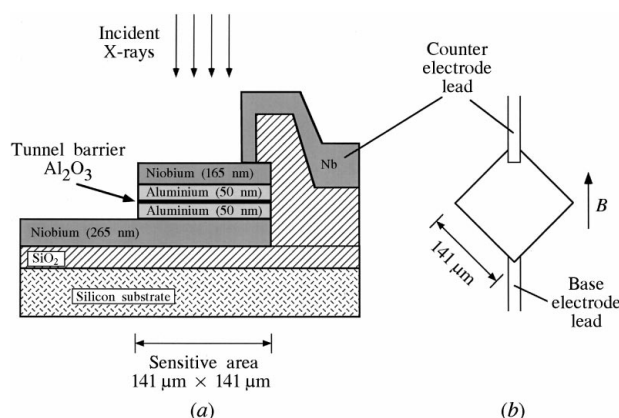
Figure 1
Schematic cross section of the STJ detector. The detector is diamond-shaped with an area of 141 × 141 μm. This detector was fabricated at Conductus Inc. using a modified photolithographic Nb trilayer process. (*a*) Cross section. (*b*) Top view.

to be about 5 eV at 6 keV incident X-ray energy (Rando *et al.*, 1992). In practice, additional statistical fluctuations associated with the trapping, tunnelling and recombination processes (Mears *et al.*, 1993; Goldie *et al.*, 1994) may degrade this limit, but a resolution of ~10 eV at 6 keV should be obtainable.

A schematic of the experimental set-up is shown in Fig. 2. The STJ detector was housed in a pumped liquid-helium cryostat equipped with an adiabatic demagnetization refrigerator (ADR) unit with a base temperature of ~50 mK. The detector was attached to a cold stage in good thermal contact with the ADR unit. During the experiments the ADR temperature was not regulated and allowed to drift up freely to ~500 mK, at which point the detector performance started to degrade. Typically, this drift occurred over a period of ~4 h. After that, the ADR unit had to be recycled, *i.e.* run through a magnetization–demagnetization cycle, which typically took ~20 min. The fluorescence sample was located on the tip of a sample holder arm which could be inserted into the cryostat and placed into the synchrotron beam through a load-lock system. During the measurements, this tip was heat sunk to the 2 K stage of the cryostat. The load-lock system allowed us to change samples in ~30 min. The distance between the sample and the detector was ~1 cm. A thin window consisting of 1000 Å parylene and 200 Å aluminium in front of the detector was used to block Auger electrons.

We used an FET-based preamplifier with fast (~500 ns) negative feedback to measure the current signal from the STJ detector. The rise time of the current pulses was limited by this amplifier to typically ~500 ns; the decay time of the current pulses was ~4–5 µs. The pulses were further amplified and shaped with a simple band-pass filter and then fed into a pulse-height analyzer without any further signal processing. The measurements reported here were performed at relatively low count rates of ~1000 counts s^{-1} to obtain optimal energy resolution. Above ~1000 counts s^{-1} a slight degradation of the resolution could be observed. During most measurements we also injected pulses with similar shape from a pulse generator into the electronics to monitor the electronic noise.

3. Results

Fig. 3 shows the X-ray fluorescence spectrum obtained with a sample consisting of boron nitride covered partially by titanium powder excited by 500 eV X-rays. This sample was chosen to simulate B and TiN, which are important materials in semiconductor fabrication. The *K* lines of B and N and the *L* line of Ti
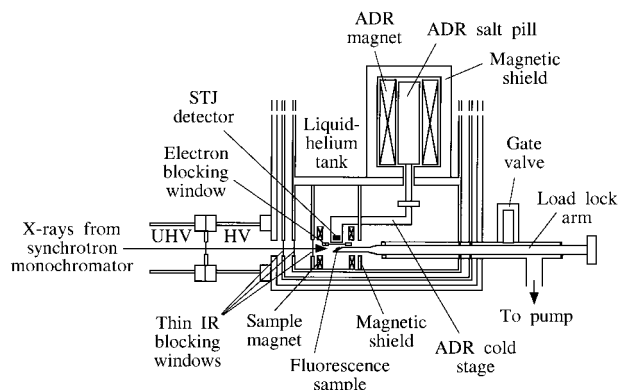
are well separated in this spectrum. Also present in this spectrum are *K* lines from C and O, presumably from oxides and contaminations in the sample, and an X-ray line at 500 eV from scattered incident X-rays. The FWHM energy resolution of the X-ray lines ranges from 9.6 eV for C *K* to 13.1 eV for Ti *L*. The electronic noise in this measurement was 6.7 eV, as indicated by the width of the pulser line. For comparison, the resolution of SiLi detectors in this energy range is about a factor of ten worse and not sufficient to separate the Ti *L* line from the N *K* line.

The *K* lines of B, C and N in Fig. 4 are each accompanied by a 'hump' of events at the low-energy side of the line labeled 'surface layer events'. These humps were also found during previous measurements in which the detector was irradiated directly with the synchrotron beam (Frank *et al.*, 1998). They probably originate from events caused by X-rays absorbed in a less responsive surface layer of our detector. Such a surface layer may be composed of niobium oxide, residues of SiO$_2$ from the detector fabrication process or other surface contaminations, and predominantly affects the lower-energy X-rays. The exact origin of these surface-layer events and the other background seen at the low-energy end of the spectrum is still under study.

Fig. 4 shows a fluorescence spectrum measured with a manganese oxide sample and an incident beam energy of 700 eV.
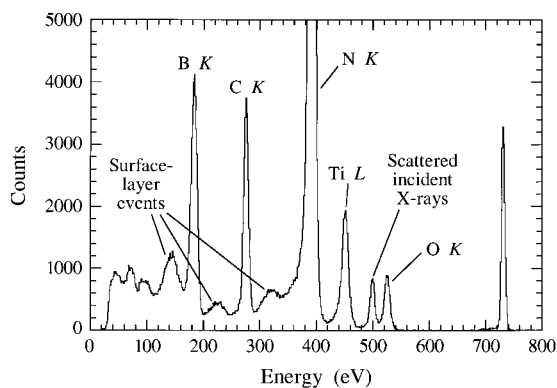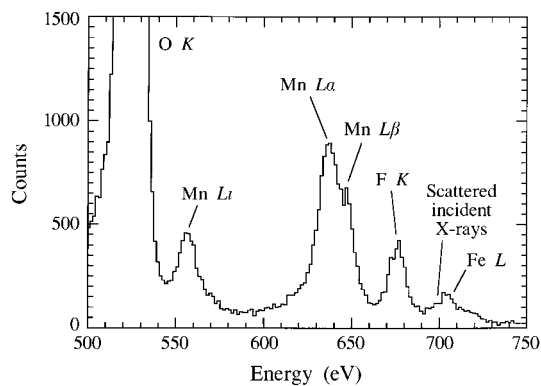

Figure 3
Fluorescence spectrum obtained with a sample consisting of boron nitride covered partially with titanium powder excited by 500 eV X-rays. The FWHM energy resolution ranges from 9.6 eV for C *K* to 13.1 eV for Ti *L*. The electronic noise was 6.7 eV.
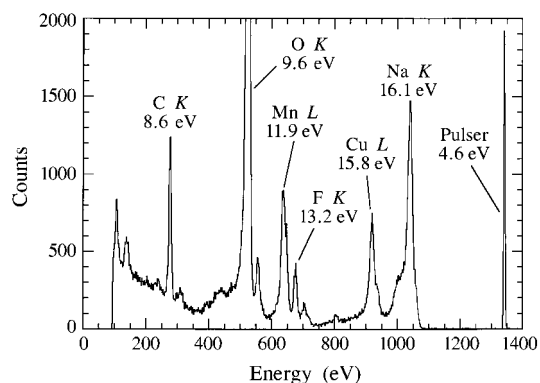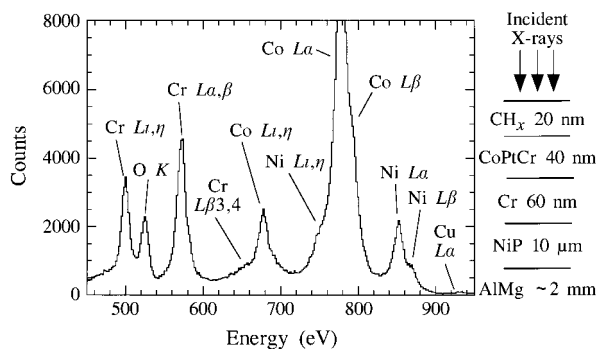

Figure 4
Fluorescence spectrum with a manganese oxide sample and an incident beam energy of 700 eV. The Mn *L* lines are well resolved from the large O *K* line. Na *K* and F *K* lines are probably due to contamination of the sample; Cu *K* and C *K* lines may originate from parts of the cryostat exposed to the incident beam. The numbers indicate the FWHM energy resolution. The electronic noise was 4.6 eV

Figure 2
Schematic diagram of the experimental set-up as discussed in the text.

The Mn *L* lines are well resolved from the large O *K* line. Other X-ray lines present in this spectrum are Na *K* and F *K*, which are probably due to contamination of the sample, Cu *K* from fluorescence of cryostat parts made of Cu, and C X-rays which may originate in the parylene Auger electron-blocking filter in front of the detector. The energy resolution in this spectrum ranges from 8.6 eV at C *K* to 16.1 eV at Na *K*. The electronic noise was 4.6 eV. An expanded part of this spectrum is shown in Fig. 5 revealing the Mn *L* lines in more detail. With the measured resolution of 11.2 eV at 640 eV, the line splitting between Mn *Lα* and *Lβ* is becoming apparent. The ability to measure Mn fluorescence in the presence of large amounts of O is interesting for various biological studies, *e.g.* the study of photosystem II, which is a protein containing Mn (Cramer *et al.*, 1992; Peng *et al.*, 1994). These measurements are very difficult with conventional detectors because of significant line overlap between O *K* and Mn *L* lines.

Fig. 6 shows part of a fluorescence spectrum measured with a sample from a magnetic storage disk fabricated by IBM with 1000 eV incident X-rays. The composition and thickness of the various metal layers in this sample are indicated on the right-hand side of this figure. Most of the *L* lines of the transition elements present in the sample (Cr, Co and Ni) are resolved from each other and indications for some substructures of the lines are visible. The resolution in the energy range shown was 10–15 eV.

Figure 5
An expanded part of the spectrum from Fig. 4 revealing the Mn *L* lines in more detail.

Figure 6
Fluorescence spectrum measured with a sample from a magnetic storage disk fabricated by IBM with 1000 eV incident X-rays. The composition and thickness of the various metal layers in this sample are indicated on the right-hand side of this figure. The energy resolution in the energy range shown was 10–15 eV.

4. Conclusions

We have demonstrated the feasibility of performing SR-XRF measurements with an STJ detector cooled to ∼100 mK coupled to a room-temperature synchrotron beamline. The measured detector resolution in the energy range 100–1000 eV was 6–16 eV. Thus, the *K* X-ray lines from the low-*Z* elements such as B, C, N, O and F and transition element *L* lines in between could largely be resolved. The measurements reported here were performed at relatively low count rates of ∼1000 counts s^{-1} to obtain the optimal energy resolution. We have recently shown that our detector can count at much higher rates up to several 10 000 counts s^{-1} with only moderate degradation of resolution. Thus, STJ detectors can approach count rates possible with semiconductor detectors while still providing a significantly better energy resolution for soft X-rays. These results indicate that STJ detectors may prove very useful in XRF and microanalysis applications studying light elements and transition metals.

References

Barfknecht, A. T., Ruby, R. C. & Ko, H. (1991). *IEEE Trans. Magn.* **27**, 3125–3128.
Booth, N. E. (1987). *Appl. Phys. Lett.* **50**, 293–295.
Booth, N. E. & Goldie, D. J. (1996). *Supercond. Sci. Technol.* **9**, 493–516.
Cramer, S. P., Chen, J., George, S. J., van Elp, J., Moore, J., Tensch, O., Colaresi, J., Yocum, M., Mullins, O. C. & Chen, C. T. (1992). *Nucl. Instrum. Methods*, A**319**, 285–289.
Frank, M., Mears, C. A., Labov, S. E., Hiller, L. J., le Grand, J. B., Lindeman, M. A., Netel, H., Chow, D., Caldara, G. & Barfknecht, A. T. (1998). *Rev. Sci. Instrum.* **69**(1). In the press.
Goldie, D. J., Brink, P. L., Patel, C., Booth, N. E. & Salmon, G. L. (1994). *Appl. Phys. Lett.* **64**, 3169–3171.
Hiller, L. J., Labov, S. E., Mears, C. A., Barfknecht, A. T., Frank, M., Netel, H. & Lindeman, M. A. (1995). *Proc. SPIE*, **2518**, 249–255.
Mears, C. A., Labov, S. E. & Barfknecht, A. T. (1993). *Appl. Phys. Lett.* **63**, 2961–2963.
Mears, C. A., Labov, S. E., Frank, M., Lindeman, M. A., Hiller, L. J., Netel, H. & Barfknecht, A.T. (1996). *Nucl. Instrum. Methods*, A**370**, 53–56.
Mears, C. A., Labov, S. E., Hiller, L. J., Frank, M., Netel, H. Azgui, F. & Barfknecht, A. T. (1995). *IEEE Trans. Appl. Supercond.* **5**, 3069–3072.
Ott, H. R. & Zehnder, A. (1996). *Nucl. Instrum. Methods*, A**370**, 1–300.
Peacock, A., Verhoeve, P., Rando, N., van Dordrecht, A., Taylor, B. G., Erd, C., Perryman, M. A. C., Venn, R., Howlett, J., Goldie, D. J., Lumley, J. & Wallis, M. (1996). *Nature (London)*, **381**, 135–137.
Peng, G., de Groot, F. M. F., Hamalainen, K., Moore, J. A., Wang, X., Grush, M. M., Hastings, J. B., Siddons, D. P., Armstrong, W. H., Mullins, O. C. & Cramer, S. P. (1994). *J. Am. Chem. Soc.* **116**, 2914–2920.
Rando, N., Peacock, A., van Dordrecht, A., Foden, C. L., Engelhardt, R., Taylor, B. G., Gare, P., Lumley, J. & Pereira, C. (1992). *Nucl. Instrum. Methods*, **313**, 173–195.
Twerenbold, D. (1996). *Rep. Prog. Part. Phys.* **59**, 349–426.